Lab on a Chip

Cite this: *Lab Chip*, 2012, **12**, 4657–4664

PAPER

Liquid alloy printing of microfluidic stretchable electronics†

Seung Hee Jeong, Anton Hagman,‡ Klas Hjort, Magnus Jobs, Johan Sundqvist and Zhigang Wu*

Received 31st May 2012, Accepted 13th September 2012
DOI: 10.1039/c2lc40628d

Recently, microfluidic stretchable electronics has attracted great interest from academia since conductive liquids allow for larger cross-sections when stretched and hence low resistance at longer lengths. However, as a serial process it has suffered from low throughput, and a parallel processing technology is needed for more complex systems and production at low costs. In this work, we demonstrate such a technology to implement microfluidic electronics by stencil printing of a liquid alloy onto a semi-cured polydimethylsiloxane (PDMS) substrate, assembly of rigid active components, encapsulation by pouring uncured PDMS on-top and subsequent curing. The printing showed resolution of 200 μm and linear resistance increase of the liquid conductors when elongated up to 60%. No significant change of resistance was shown for a circuit with one LED after 1000 times of cycling between a 0% and an elongation of 60% every 2 s. A radio frequency identity (RFID) tag was demonstrated using the developed technology, showing that good performance could be maintained well into the radio frequency (RF) range.

Introduction

Today, user experience and acceptance are strongly influencing innovations, and hence product design and technology development. For example, user-friendly man–machine multi-touch interfaces have reinvented smart phones and tablets, which makes Internet information available almost everywhere and at any time.

In electronic technology, a new revolutionary technology concept has been proposed with many highly attractive new features already demonstrated – stretchable electronics – targeting conformal attachment on bodies[1] with various strategies.[2–7] For example, recently the Rogers group at University of Illinois, Urbana-Champaign, demonstrated the so-called epidermal electronics.[2] Being mechanically unnoticeable to the user (much like a temporary tattoo), the presented devices conformally attach to the human skin and can measure various physiological signals, such as electroencephalograms, electrocardiograms, and electromyograms, with potential to communicating data wirelessly. Ultimately, this kind of device may greatly improve man–machine interface, fitness monitoring, home care of the elderly, and health and clinical monitoring.

Complementary to the elastic electronics that is based on integrated circuit (IC) technology, stretchable printed electronics allows for larger areal stretchable circuits at lower costs. One example is based on microfluidics[8] by introducing a liquid alloy into micro replicated channels, liquid conductors and other viscous components embedded into stretchable materials such as silicones.[9–13] Due to its fundamental advantage of being well suited for designing large cross-sections, some passive components that demand low electrical resistance, such as longer interconnects,[10] larger antennas[11–13] and sensors,[14] were demonstrated using this technique. To allow for high performance, rigid active components in microfluidic based stretchable electronics, we have proposed a new concept of hybrid stretchable electronics at a device level. Rigid active components were integrated and encapsulated onto microfluidic passive components within localized stiff cells (LSCs).[15] Using this technique, a standalone radio frequency (RF) radiation sensor[15] and a reversibly stretchable large-area wireless strain sensor[16] have been demonstrated. Furthermore, microfluidic approaches have been studied by other groups for deployment of non-linear components such as tunnel junctions[17] and memristors,[18] as well as electrochemical energy handling components,[19] for energy harvesting[20,21] and batteries.[22]

However, the fabrication techniques for microfluidic stretchable electronics is still at a laborious handicraft stage with serial injection of the liquid at low throughput and reliability, which is far away from a fabrication process suitable for systems used in applications such as interactive gaming, wearable computing, healthcare or fitness monitoring, medical diagnostics, and epidermal electronics. Hence, a robust and reliable parallel process is needed for the device and system development of stretchable/conformal microfluidic electronics. In this work, such a technology was developed. The microfluidic stretchable electronics was implemented by stencil printing of a liquid alloy onto a semi-cured polydimethylsiloxane (PDMS) substrate, assembly of rigid active components, and subsequent encapsulation by

Department of Engineering Sciences, Uppsala University, Box-534, The Angstrom Laboratory, SE-751 21, Uppsala, Sweden. E-mail: Zhigang.Wu@angstrom.uu.se
† Electronic supplementary information (ESI) available. See DOI: 10.1039/c2lc40628d
‡ Current address: KTH, Hållfasthetslära, Osquars backe 1, SE-100 44, Stockholm, Sweden

pouring PDMS pre-polymer and curing. The printing resolution and the resistance of the liquid conductors were investigated. Finally, a radio frequency identity (RFID) tag was fabricated and demonstrated with the proposed fabrication technique.

Principles and design

As discussed previously,[8,15] one of the feasible solutions to make microfluidic stretchable electronics is to adopt LSCs. In this approach, highly capable active components with small footprint were encapsulated in the large areal stretchable microfluidic system, where its surrounding is made mechanically stiffer and well protected, to achieve an overall stretchability of the whole device, although the rigid active components cannot be stretched at all. Based on this concept, we propose a solution to deploy a parallel technology for microfluidic stretchable electronics, as illustrated in Fig. 1. Basically, first an elastic foil is prepared as a substrate, Fig. 1(a); secondly liquid alloy circuits serving as either connectors or components are printed on the substrate to form a microfluidic circuit, Fig. 1(b); thirdly, rigid components/ICs/circuitry, are mounted onto the circuit, Fig. 1(c); fourthly, the device is closed by covering a second layer of elastic material, Fig. 1(d); and finally LSCs are made to minimize the stress in the areas containing rigid components.[15]

Considering the fact that (a) the thin oxidized layer of gallium based liquid alloys is solid and mechanically rather stiff,[23–26] and that (b) silicones such as PDMS can both serve as a substrate and a packaging material, the approach we proposed above is feasible if we can successfully pattern such a liquid alloy on an elastic substrate. Hence, the critical part is how to introduce the liquid alloy in a parallel way. Printing is a viable alternative in electronic industries and widely used for production of miniaturized, robust and low-cost electronic circuits or disposable chemical sensors. In this work, a stencil printing technique was proposed to print the liquid alloy on a semi-cured elastic substrate, Fig. 2.

Briefly, first the liquid alloy is casted evenly onto the surface of a silkscreen (or a similar flexible carrier), meanwhile a semi-cured PDMS substrate is prepared on a hard flat and smooth support; then a suitable stencil is put on the semi-cured substrate, and the liquid alloy is lowered to the substrate *via* the openings of the stencil by applying a normal force through the silk screen; in a third step the liquid alloy is made thicker and evenly in the stencil by rolling with liquid alloy on the roller; and finally, the liquid

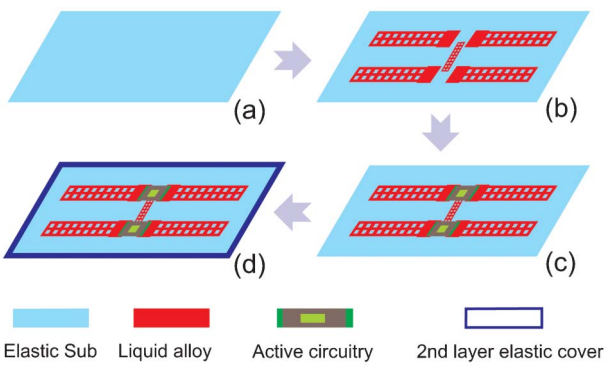

Fig. 1 Schematic of the proposed parallel technology for microfluidic stretchable electronics.

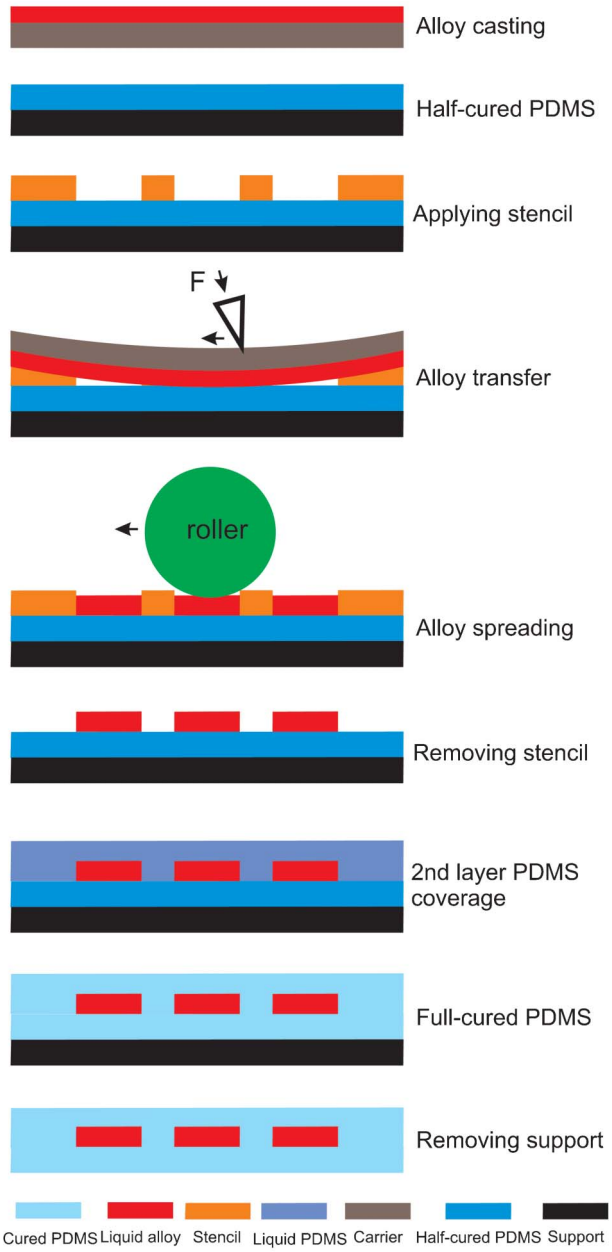

Fig. 2 Schematic of the fabrication process.

alloy patterns are obtained by removing the stencil. If a pure liquid alloy circuit is intended, this is followed by covering the liquid alloy with uncured PDMS and fully curing all PDMS. The final circuit is obtained by peeling it from the support. If active components are to be integrated, the components and external interconnects are put on the liquid alloy by a pick and place machine before the second PDMS layer is poured over the circuit.

Materials and methods

PDMS preparation

Unless stated otherwise, the PDMS Elastosil® RT601 from Wacker, was mixed in a 9 : 1 weight ratio (base : cross-linker).

To remove the air bubbles and prolong the time span that can be used, the PDMS was mixed in a plastic cup and then put to rest in a standard freezer at −18 °C.

The support, on which the PDMS substrates were cast, varied from oxidized pre-cast PDMS frames to 4" Si-wafers and plastic Petri dishes. In most of the tests the back of a plastic Petri dish (84 mm in diameter from VWR international) was used. Alternatively, a Laurel WS400B-6NPP-Lite spin coater was used to obtain high uniform substrates. On all supports, the desired amount of PDMS was poured/spin-coated and then spread out by blowing with compressed nitrogen gas. Afterward, the sample was resting in a standard household fridge at ≈4 °C to form an even thickness. The treatment with nitrogen gas and fridge cooling also removed any lasting air bubbles from the PDMS. All oven curing was done in a Memmert UM 400 convection oven at ≈74 °C unless otherwise stated.

Liquid alloy patterning and device fabrication

A copper stencil mask is placed on the substrate. The stencil mask should be in full contact with the substrate. A screen with a thin layer of the liquid alloy Galinstan (Geratherm Medical AG) is lowered onto the stencil mask, after which a squeegee is stroked on the upside of the screen to press the Galinstan on the screen into contact with the substrate through the pattern in the stencil mask. This first step with the screen is performed to get a laterally well-defined "sticking" layer on the substrate. After the screen has been removed, a Galinstan covered roller is rolled over the mask. This step makes the print thicker and more even in thickness. After the rolling, the stencil mask was removed and the print was done. These steps and the placing of the components were preferably done as fast as possible, since the substrate was still curing (although at a lower rate). The time window (≈1 h) could be expanded by cooling the substrate and consequently decelerate the curing rate. The reason for making the initial print with a screen, instead of the doctor's blade or roller technique, was that the print made with the screen had better coverage and less risk of damaging the mask pattern.

After printing, surface mount devices (SMD) might be placed on the print with a pick and place machine from LPKF. These components have to be placed on the surface with a downward motion perpendicular to the surface, otherwise the prints might get smudged. When the components had been placed, uncured PDMS was carefully poured onto the substrate covering the circuit. If no components are present, it is possible to even out and reduce the thickness of the uncured PDMS by blowing on it with compressed air or nitrogen gas. When the PDMS had been dispensed it was placed in a fridge to rest, in order to become smoother and release air bubbles captured in the PDMS. When rested, the substrate was placed in an oven to fully cure and to bond to the lid. The final curing could be done at a suitable temperature.

For the investigation of the printing method, a screen-printing silk screen with a 100 threads/in mesh was used. As a squeegee for distributing Galinstan to the screen, a simple ice rake was used. Homemade squeegees of PDMS were used for pressing down the screen to the substrate through the copper stencil mask. All stencil masks were made from a 50 μm copper foil that was wet etched in a copper etchant from ELFA, Sweden. The copper had been patterned by standard UV lithography with a plastic transparency mask. The roller was made of foam rubber and bought from a hobby-material supplier. For length and thickness measurements a standard Vernier calliper or micrometre screw was used.

To verify the integration of active components, Kingbright red and orange light-emitting diodes (LEDs) with package size of 0603 from Farnell were assembled to liquid alloy circuits. For device demonstration, an ultra-high frequency (UHF) RFID tag was made by assembling a packaged RFID chip (Higgs-3, Alien technology) onto a microfluidic antenna and a measuring with a reference antenna design from the same provider.

Electrical measurements and evaluations

PDMS can be assumed to have a Poisson's ratio close to 0.5,[27] *i.e.*, it volume does not change during low stretch. At higher stretch the behaviour is more complicated. A channel inside a PDMS body will follow the changes in the body as a whole and if the channel is filled with a more or less incompressible fluid it will keep its volume. Hence, the changes in length, width and height of the encapsulated liquid should follow the corresponding changes in the whole body; although at large strains the incompressibility might force the PDMS to adapt in order to let the fluid keep its volume.

As a conductor, the channel filled with liquid alloy can be seen as a normal solid one, for which the following equation applies:

$$R = \rho L/A \tag{1}$$

where R is the electrical resistance, A is the cross section area, L is the length and ρ is the resistivity of the alloy (43.5×10^{-8} Ωm). The resistance for conductors in series R_s, is the sum of the serially connected resistances R_1 to R_n. Using eqn (1) and knowing the basic geometry of the sample, the height of the channels could be estimated by assuming that they have a homogeneous height.

To enable resistance measurements on covered prints, bent copper foil pieces were attached to the print before they were covered by the second layer of PDMS. The copper pieces were

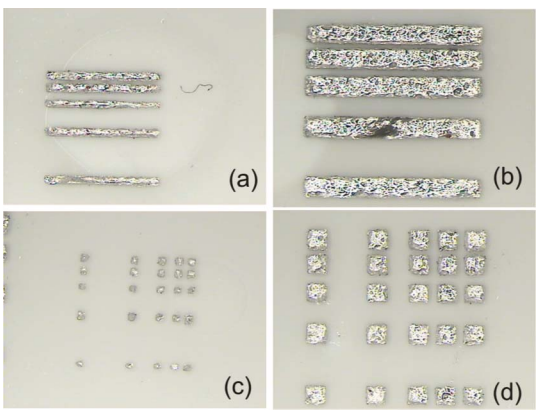

Fig. 3 Photos of the lateral resolution of the lines and squares: (a) 200 μm wide lines with spacings from 100 to 1000 μm; (b) 500 μm wide lines with spacings from 100 to 1000 μm; (c) Squares 200 μm sides, with spacings from 100 to 1000 μm; and (d) Squares 500 μm sides, with spacings from 100 to 1000 μm.

formed in such a way that they reached above the surface of the uncured PDMS. After the sample had been cured, small wires were soldered onto the copper plates to simplify handling. A computer connected Agilent 34405A digital multimeter was attached to the wires for recording the resistances. This setup was used to cycling stretching tests as well to verify the mechanical reliability preliminarily.

All stretch tests were conducted in a Plexiglas frame, Fig. S1, ESI.† The samples were either clamped into the frame directly or bonded to glass slides, which in turn were clamped into the frame. The amount of stretch was measured with a couple of mm graded rulers that were attached to the frame.

For the stretchable UHF RFID antenna evaluation a balanced-unbalanced transformer (900 MHz, Johanson technology) for conversion from differential to single line feed and matching impedance of the prepared UHF RFID antenna was connected to both sides of a liquid metal alloy antenna and a coaxial cable of a network analyser through an SMA (SubMiniature version A) connector. For this connection, short wires were implemented through PDMS top layer from liquid metal alloy antenna before the cover layer was finally cured. The prepared antenna performance was tested with a network analyser (E8364B, PNA series network analyser, Agilent), Fig S2, ESI.† The UHF RFID antenna was manually stretched in a specially designed jig structure up to 40% length change from the initial dimensions to the direction of each side of rectangular shape antenna, respectively, for getting an RF signal change of resonant frequency and reflection coefficient from 100 MHz to 1.5 GHz.

The tests on RFID reader responsitivity performance were also conducted with a commercial RFID reader (Speedway Revolution R420, Impinj) connected to an 865–868 MHz frequency range antenna (8 dB_{ic} RHCP, S8658PRJ, Laird technologies). The experiment was set up to exhibit real operation ability of the stretchable UHF RFID tag from 2 m to 14 m distance, Fig. S3, ESI.† Reading quality and successful package transmission between reader and tag was evaluated, where the reader was at 14 m distance from the stretchable RFID tag when it was stretched up to 40% of initial length in two orthogonal directions. The reading quality between the reader's antenna and the stretchable UHF RFID tag was recorded as RSSI (received signal strength indicator) level in the monitoring software (Speedway revolution, Impinj) provided by the same provider. The number of successful tag interrogations per second was calculated from measured data gathered during 1 min. The transmission power from the reader's antenna was 30 dB_m and the cable length from the reader to it was 2 m.

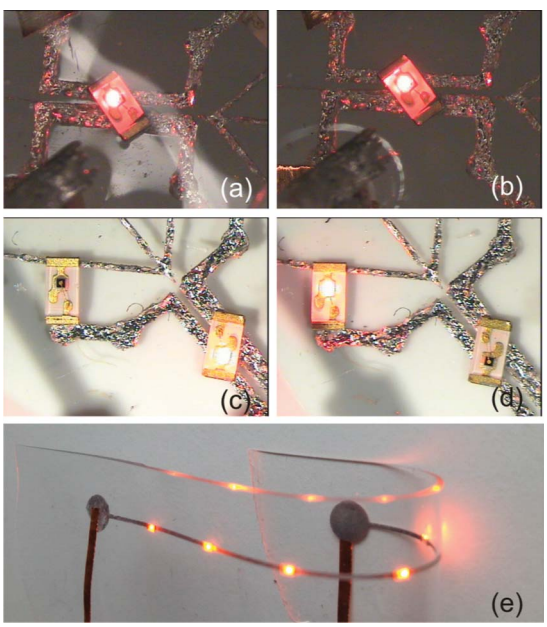

Fig. 4 Photos of the integrated LEDs. One LED integrated while non-stretched (a) and 10% stretched along horizontal direction (b). Two series connected LEDs while the right one is on (c) and the left one is on (d). Five serial connected LEDs (e).

Results and discussion

PDMS preparation

Initial experiments with uncured PDMS pouring on cured PDMS substrates showed that the adhesion was best for dry untreated surfaces. Although it might appear to be properly bonded to a substrate, the two layers were easy to peel off each other if a good hold could be established to the different layers. The adhesion was best at the edges of a layer and, to some degree, at the corners of channels. If the surface was cleansed with solvents (*e.g.* ethanol or iso-propanol alcohol) the adhesion was reduced (probably due to residues on the surface). Furthermore, the adhesion became distinctly worse if the substrate surface was oxidized with a corona discharge treatment prior to the "bonding". It was concluded that uncured PDMS mixture does not bond well to cured PDMS.

Uncured PDMS will, however, bond to uncured PDMS, and semi-cured PDMS will bond to semi-cured PDMS and as it turned out; uncured PDMS bonds to semi-cured PDMS. However the substrate needs to be fairly rigid to be printed upon. Together these two demands, a substrate being hard enough to be printed on and being uncured enough to bond to uncured PDMS, forms the boundaries of a time window that decides how long a substrate should be cured before being printed on. The length of this window and where it occurs

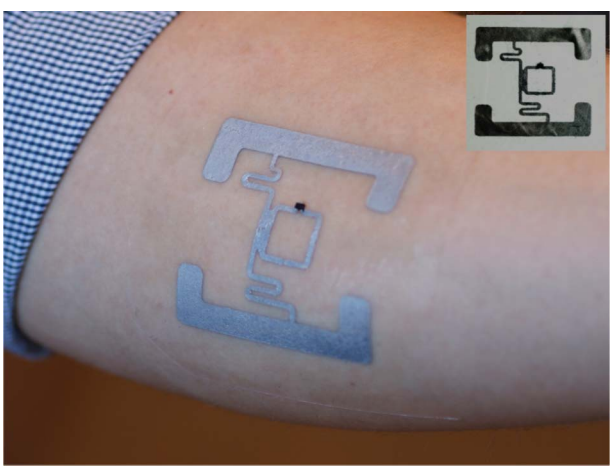

Fig. 5 Photo of the demonstrated stretchable/conformable UHF RFID tag.

depend on the PDMS blend, the substrate dimensions, the support on which the substrate lies and the curing temperature with time. The PDMS in itself has different curing behaviour dependent on mixing ratio, sub-type and composition (differs between different manufactures). As for the substrate dimension it is mainly the thickness that plays a role, due to the slow heat transfer. If a thick substrate is cured at high temperatures the surface is cured faster than the bulk, which in the worst case results in a surface that is fast cured to be bonded (to uncured PDMS) above an almost liquid core. The type of substrate support used affects the substrate in a similar way (*e.g.* a sample taken from a fridge and put into an oven cures faster and more evenly if it is on a thin plastic support than on thick glass). As for the curing temperature, a lower temperature slows down the curing rate. Furthermore, a slower curing rate evens out the temperature throughout the substrate, which in turn results in a more evenly cured substrate (and similarly for different supports).

As an example, one gram of PDMS (1 : 9) evenly spread out over the backside of a plastic Petri dish (84 mm diameter, 0.3 mm thickness) cured at 74 °C should be cured for 3 min 40 s ($\pm$ 10 s). If it is cured longer the adhesion to uncured PDMS suffers; if it is cured for a shorter time the copper mask will stick to the substrate and may rip it apart when lifted.

Line width, height and space testing

Prints were successfully carried out on substrates of down to 0.2 mm thickness (with a spin-coater) and with a similarly thin cover layer; test samples with a total thickness of 0.4 mm were achieved. The lateral extension of the samples varied since it is dependent on how the mask and support structure were designed. As for maximum thickness, no explicit test was done, but samples as thick as 3 mm have been made. Furthermore, printing in two layers was successfully tested. This was achieved by pre-curing the lid and using it as a substrate layer (repeating the process one more time). These multilayer tests were carried out without components, outside connections, or vias between the different layers.

As for the lateral printing resolution, a line with of 200 μm with separation of 100 μm was achieved. Squares with an edge length of 200 μm were also demonstrated. Circuit paths with liquid conductors approximately 200 μm wide with distances of 100 μm where successfully printed. However, a severe problem was that the durability of the copper stencil mask is reduced when there are many fine and complicated patterns. Also, a taunting limitation of stencil printing is that all metal needs to be connected in the opening of the stencil mask, which limits the potential complexity of any circuits. Resulting structures from the resolution tests can be seen in Fig. 3.

Components integration and device demonstration

Several experiments with simple components such as LEDs were conducted. It showed a good electrical performance while still remaining stretchable to some extent, *e.g.* the LEDs in Fig. 4(a,b). Up to five LEDs were connected in series and fully functional in parallel and serial line configurations to connect LED pads, *e.g.* the LEDs in Fig. 4(c–e). The experiences from LED integration were transferred to make a UHF RFID tag, which measured around 45 × 43 mm. Fig. 5 shows one tag that was conformally mounted on the human skin. In addition, part of the electrical performance of its printed microfluidic antenna has been measured, Fig. S4, ESI.†

A complete UHF RFID tag, chip and antenna, could be read at a distance up to nearly 14 m (13.95 m) in ambient air from the reader antenna when the tag was unstretched in upright position and at a distance of 8 m when it was rotated by 90°, Fig. 6(a). The difference in reading range is believed to stem from the non-isotropic radiation pattern of the tag antenna and, to some extent, from the polarization of the reader antenna.

With the UHF RFID tag in an upright position and placed 14 m from the reader antenna, the tag was stretched in two different directions while the reader's maximum received signal strength indicator (RSSI) value was measured. The result, Fig. 6(b), shows that a small amount of stretching in the *y*-direction actually improves the received signal strength whereas stretching in the *x*-direction decreases it. The effect of

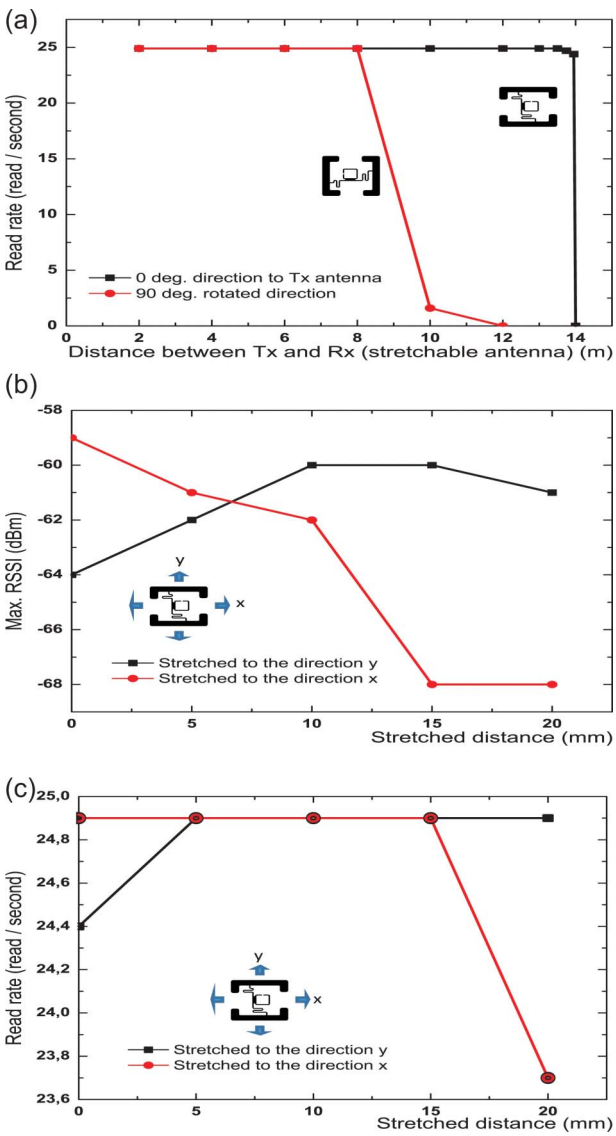

Fig. 6 Demonstrated performance of the printed microfluidic UHF RFID tag.

this is also shown in Fig. 6(c), where it can be seen that the read rate is increased when the tag is stretched in the *y*-direction, whereas it decreases when the tag is stretched too far in the *x*-direction. Since the non-stretched antenna had a resonance centre frequency of 885 MHz and the resonance frequency decreases when stretched, a certain amount of stretch will shift the resonance centre frequency to the same as the reader antenna is transmitting, 868 MHz. From these measurements, it can be seen that this is happening at 10–15 mm stretch in the *y*-direction. The shift in antenna resonance is due to both a change in geometry of the resonating structure as well as changing the characteristic impedance of the integrated matching network. Both these parameters affect the power radiated from the complete tag.

In summary, the measurements on a UHF RFID tag proved that our concept works well, although deeper investigations are required for future development. For example, optimization for body area network components on the human body should be evaluated.

Stretching behaviours

A Galinstan circuit without any components or connections can be stretched to 100% elongation without breaking. Circuits with rigid components have been successfully stretched to 60% elongation without breaking, when a spin-coater was used to prepare the samples. The measured results from seven different samples are shown in Fig. 7. We manually examined the cycled samples 1000 times (0.5 Hz) between 0% and 20%, 40% and 60% elongation respectively, Fig. 8. However, the results were not conclusive and more experiments with a dedicated tensile tester or similar are needed. Some of the samples did not pass the cycling tests. In those cases, the rapture usually started at a rigid component (at the corner of it) or at the measurement contacts of copper sticking out of the PDMS. The reduced robustness mainly came from stress concentration or thinner cross-section area at the location of a chip or a lid without properly prepared LSCs. In the current experiments, the LSC was formed by manually dropping a tiny PDMS droplet on the device or copper contact, which was difficult to repeat precisely. Further

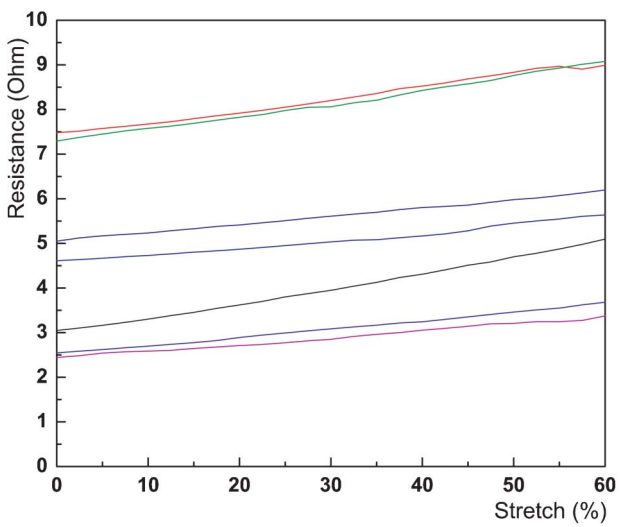

Fig. 7 Measured resistances without LED from 7 samples.

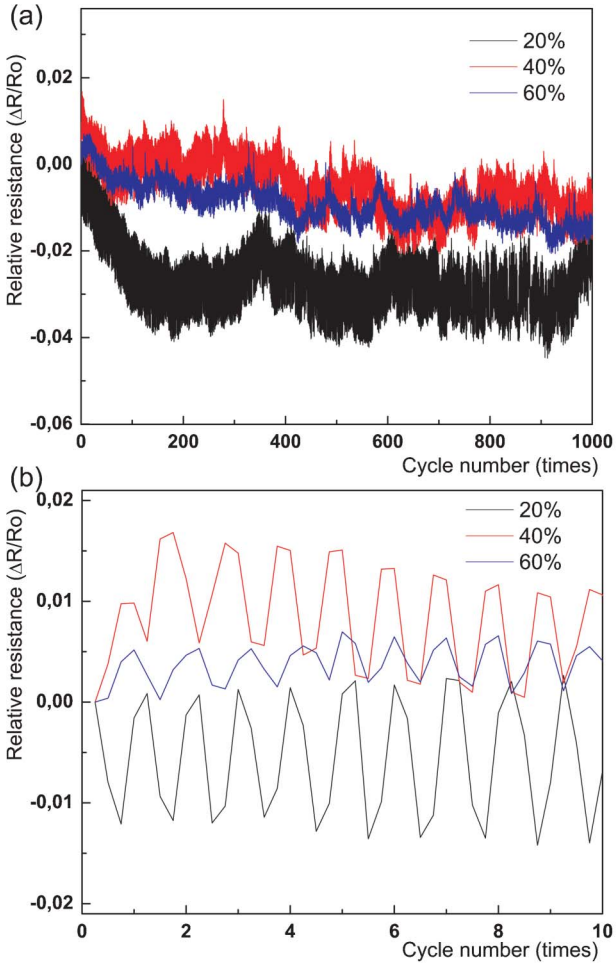

Fig. 8 Measured relative resistance while stretch cycling at different elongations of a simple liquid alloy circuit with a LED integrated between two 11 mm long liquid conductors. The thickness of the PDMS is 550 μm except LSCs. (a) data for 1000 cycles; (b) data from the first 10 cycles.

mechanical study and optimization of the shape, thickness, size, and Young's modulus of the LSCs would significantly benefit the reliability of the integrated devices. In a recent publication, 600 000 bending cycles were achieved at a maximum strain of 40% in a circuit combining liquid alloy and thin film gold (by injecting Ganlinstan into a PDMS microchannel network – like in previous works of ours – on a polyimide foil with thin film gold).[28] Although without any rigid components integrated in the circuit, it indicates a good potential for our technology to reach long-term reliability.

When cycling of stretchable samples were progressed, the resistance of liquid metal line was slightly reduced with increased number of cycle times. However, afterwards when the samples were rested around 20 min, the resistance went up slightly higher than the initial value before the cycling experiments. We have not figured out what was the reason for this reduced resistance. The circuits without components did not show any reduced resistance after being stretched, Fig. S5, ESI.† One possible explanation is that it is from the contacts between the components and liquid alloy, *e.g.*, from opening the oxide layer at the contacts.

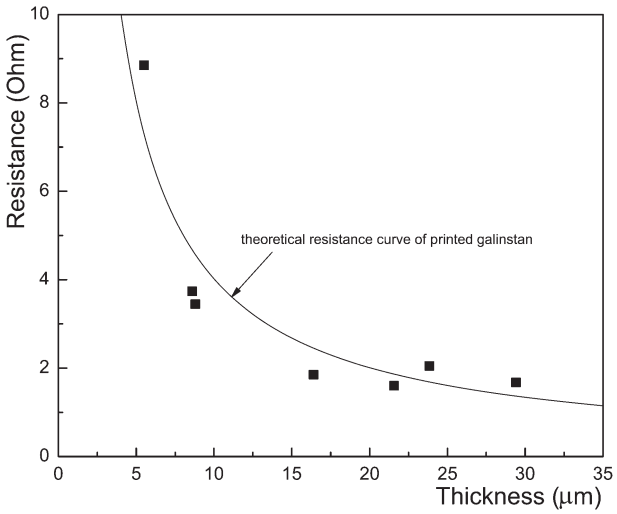

Fig. 9 Expected and measured resistances when unstretched. The printed Galinstan line is 60 mm long and 0.65 mm wide.

Comparing the simple modelling and measured resistances of un-stretched samples, the height estimation can be seen in Fig. 9. The results indicate an average height between 6 and 30 μm. This seems plausible, considering that the photos taken indicate that the Galinstan layer is thinner than the 50 μm thick copper stencil mask before lifting away the stencil.

Discussion on liquid alloy handling

Three features dominate the behaviour of Galinstan in the fabrication processing. It has a very low viscosity (2.4 mPa·s), which is helpful when transporting the liquid. Also, it has a very high surface tension (718 mN m^{-1}). With such a high surface tension, it tends to adhere to most surfaces, *e.g.*, most metals, ceramics, and plastics. It provides an extraordinary advantage in the good wetting between the liquid alloy and its elastic substrate. However, it was a huge challenge to transfer the liquid alloy while avoiding contamination, which has commonly been regarded as one of the two nuisances of gallium-based alloys.[8] The last one is that this kind of liquid alloy is always covered by a thin solid layer of oxides.

Concerning the printing technology present in this article, the first issue relates to the thickness control of the liquid alloy. In our experiments, the liquid alloy was cast onto the flexible carriers such as screen silk and common office used transparency. Due to the low viscosity of the liquid alloy, the thickness on the carrier was limited to some tens of microns. Furthermore, when the carrier was separated from the substrate, the peeling force, speed, and angles cannot be well controlled during our current experiments in a handy craft state. Hence, we obtained a large variation in thickness and therefore variations in resistance even in a same series of samples made in similar conditions, Fig. 7 and Fig. 9. What's more, the high surface tension of the liquid alloy makes it stick to the carriers and the stencils. After deposition to the masked substrate, a large amount of liquid alloy is still attached to the carrier, which decreases the possible thickness of liquid alloy that we can achieve on the elastic substrate. The porous roller used to spread out the alloy in the mask openings is another reason for a high surface roughness. Finally, sticking to the stencil mask reduces further the uniformity both in thickness and width of the transferred liquid alloy circuits on the substrate. A rough surface could be observed in the demonstrated samples such as those in Fig. 3 and 4. Here, the liquid alloy keeps this rough surface is most probably because of its stiff oxide layer on its surface, *cf.* flow behaviour studies of gallium-based alloys.[25]

Due to the fact that the Galinstan sticks to the stencil, the obtained width of patterned liquid alloy circuit is always less than that of the stencil. Fig. 10 shows one of the examples for which we tried to achieve a line width of 100 μm. Irregular distribution of the liquid alloy residuals could be easily observed, Fig. 10(b) and variations in the liquid circuit width could also be found, Fig. 10(c). In extreme cases, it would lead to breakage of liquid circuits (not shown here). Although having a printing technology in its infancy, decent resolution is possible. As we show in Fig. 3, lines and square dots with a width of 200 μm could be achieved with various spaces from 100 μm.

Last but not least, the technique we present here has high potential to be improved. Suggested studies could be: 1) to seek new materials for flexible carriers and stencil masks to reduce the sticking of the liquid alloy; 2) to automate the process with well controlled conditions such as in peeling speed and lifting angle during removal of carrier and stencil; 3) the deposition of Galinstan in a reducing atmosphere to allow it to flow and avoid any surface roughness before oxidizing its surface. Finally, optimization on LSC and its fabrication will improve the life time and stretchability, with knowledge from micromechanics and interactions between the components and liquid alloy.

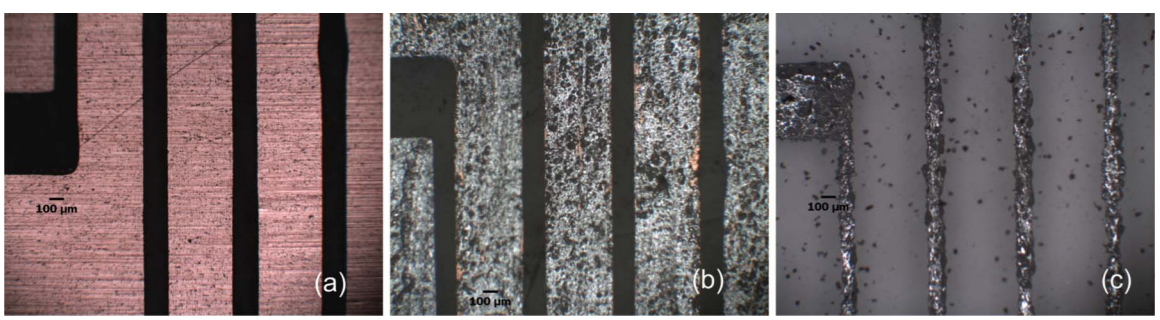

Fig. 10 Optical photographs on copper stencil mask (a) back side, (b) top side (used mask), and (c) corresponding patterned liquid alloy on elastic substrate using this copper mask.

Conclusions

In this work, a parallel processing technology has been demonstrated to implement microfluidic electronics by stencil printing of a liquid alloy onto a semi-cured PDMS substrate, assembly of rigid active components, and subsequent encapsulation by pouring uncured PDMS and curing. Line widths and separation down to 200 and 100 μm, respectively, were achieved. The active components were integrated as well with a reasonably good performance after 1000 stretching cycles between 0% and 60% elongation. Finally, by using the developed technology a UHF RFID tag was demonstrated with high signal quality. Potentially, in the future this could be a useful technique for complex large areal stretchable printed electronic systems.

Acknowledgements

The authors thank Prof. Anders Rydberg, Uppsala University, for kindly providing his facility for antenna evaluations. This work is partly funded by the Swedish Governmental Agency for Innovation Systems, through Uppsala Vinnova Excellence Center for Wireless Sensor Networks. Z.G. Wu holds a tenure track position funded by the Swedish Research Council (Contract No. 621–2010-5443).

References

1 J. A. Rogers, T. Someya and Y. Huang, *Science*, 2010, **327**, 1603–1607.
2 D.-H. Kim, N. Lu, R. Ghaffari, Y.-S. Kim, S. P. Lee, L. Xu, J. Wu, R.-H. Kim, J. Song, Z. Liu, J. Viventi, B. de Graff, B. Elolampi, M. Mansour, M. J. Slepian, S. Hwang, J. D. Moss, S.-M. Won, Y. Huang, B. Litt and J. A. Rogers, *Nat. Mater.*, 2011, **10**, 316–323.
3 D.-H. Kim, N. Lu, R. Ma, Y.-S. Kim, R.-H. Kim, S. Wang, J. Wu, S. M. Won, H. Tao, A. Islam, K. J. Yu, T.-I. Kim, R. Chowdhury, M. Ying, L. Xu, M. Li, H.-J. Chung, H. Keum, M. McCormick, P. Liu, Y.-W. Zhang, F. G. Omenetto, Y. Huang, T. Coleman and J. A. Rogers, *Science*, 2011, **333**, 838–843.
4 S. P. Lacour, J. Jones, S. Wagner, T. Li and Z. G. Suo, *Proc. IEEE*, 2005, **93**, 1459–1467.
5 I. M. Graz and S. P. Lacour, *Org. Electron.*, 2010, **11**, 1815–1820.
6 T. Sekitani, Y. Noguchi, K. Hata, T. Fukushima, T. Aida and T. Someya, *Science*, 2008, **321**, 1468–1472.
7 D. Brosteaux, F. Axisa, M. Gonzalez and J. Vanfleteren, *IEEE Electron Device Lett.*, 2007, **28**, 552–524.
8 S. Cheng and Z. G. Wu, *Lab Chip*, 2012, **12**, 2782–2791.
9 A. C. Siegel, S. S. Shevkoplyas, D. B. Weibel, D. A. Bruzewicz, A. W. Martinez and G. M. Whitesides, *Angew. Chem., Int. Ed.*, 2006, **45**, 6877–6882.
10 H.-J. Kim, C. Son and B. Ziaie, *Appl. Phys. Lett.*, 2008, **92**, 011904.
11 S. Cheng, A. Rydberg, K. Hjort and Z. G. Wu, *Appl. Phys. Lett.*, 2009, **94**, 144103.
12 J. H. So, J. Thelen, A. Qusba, G. J. Hayes, G. Lazzi and M. D. Dickey, *Adv. Funct. Mater.*, 2009, **19**, 3632–3637.
13 M. Kubo, X. Li, C. Kim, M. Hashimoto, B. J. Wiley, D. Ham and G. M. Whitesides, *Adv. Mater.*, 2010, **22**, 2749–2752.
14 Y.-L. Park, B.-R. Chen and R. J. Wood, *IEEE Sens. J.*, 2012, **12**, 2711–2718.
15 S. Cheng and Z. G. Wu, *Lab Chip*, 2010, **10**, 3227–3234.
16 S. Cheng and Z. G. Wu, *Adv. Funct. Mater.*, 2011, **21**, 2282–2290.
17 R. C. Chiechi, E. A. Weiss, M. D. Dickey and G. M. Whitesides, *Angew. Chem., Int. Ed.*, 2008, **47**, 142–144.
18 H-.J. Koo, J-.H. So, M. D. Dickey and O. Velev, *Adv. Mater.*, 2011, **23**, 3559–3564.
19 M. Kaltenbrunner, G. Kettlgruber, C. Siket, R. Schwödiauer and S. Bauer, *Adv. Mater.*, 2010, **22**, 3065–2067.
20 D. J. Lipomi, B. C-K Tee, M. Vosgueritchian and Z. Bao, *Adv. Mater.*, 2011, **23**, 1771–1775.
21 T. Krupenkin and J. A. Taylor, *Nat. Commun.*, 2011, **2**, 448.
22 Y. Yang, S. Jeong, L. Hu, S. W. Lee and Y. Cui, *Proc. Natl. Acad. Sci. U. S. A.*, 2011, **108**, 13013–13018.
23 M. J. Regan, P. S. Pershan, O. M. Magnussen, B. M. Ocko, M. Deutsch and L. E. Berman, *Phys. Rev. B: Condens. Matter*, 1997, **55**, 15874.
24 N. B. Morley, J. Burris, L. C. Cadwallader and M. D. Nornberg, *Rev. Sci. Instrum.*, 2008, **79**, 056107.
25 M. D. Dickey, R. C. Chiechi, R. J. Larsen, E. A. Weiss, D. A. Weitz and G. M. Whitesides, *Adv. Funct. Mater.*, 2008, **18**, 1097–1104.
26 R. C. Chiechi, E. A. Weiss, M. D. Dickey and G. M. Whitesides, *Angew. Chem., Int. Ed.*, 2008, **47**, 142–144.
27 J. E. Mark, *Polymer Data Handbook*, Oxford University Press, London, 1999.
28 R. Surapaneni, Y. Xie, K. Park and C. Mastrangelo, *Procedia Eng.*, 2011, **25**, 124–127.

